Applied Catalysis B: Environmental 219 (2017) 101–108

Contents lists available at ScienceDirect

Applied Catalysis B: Environmental

journal homepage: www.elsevier.com/locate/apcatb

NH_2-MIL-125(Ti)/graphitic carbon nitride heterostructure decorated with NiPd co-catalysts for efficient photocatalytic hydrogen production

Jixiang Xu, Jianyang Gao, Chao Wang, Yu Yang, Lei Wang *

Key Laboratory of Eco-Chemical Engineering, Ministry of Education, State Laboratory of Inorganic Synthesis and Applied Chemistry, College of Chemistry and Molecular Engineering, Qingdao University of Science and Technology, Qingdao 266042, China

ARTICLE INFO

Article history:
Received 12 May 2017
Received in revised form 9 July 2017
Accepted 16 July 2017
Available online 18 July 2017

Keywords:
Photocatalysis
Ti-containing MOF
Graphitic carbon nitride
NiPd co-catalysts
H_2 production

ABSTRACT

In this study, a highly efficient photocatalyst, NH_2-MIL-125(Ti)/g-C_3N_4/NiPd (NH_2-MIL-125(Ti)/CN/NiPd), was successfully synthesized for photocatalytic water reduction to produce H_2. Under visible-light irradiation, the prepared NH_2-MIL-125(Ti)/CN/NiPd composite clearly showed enhanced photocatalytic performance for H_2 evolution compared to NH_2-MIL-125(Ti), NH_2-MIL-125(Ti)/CN, and NH_2-MIL-125(Ti)/NiPd. The as-synthesized NH_2-MIL-125(Ti)/0.75CN/$Ni_{15.8}Pd_{2.1}$ photocatalyst exhibited a high H_2 production rate of 8.7 mmol g^{-1} h^{-1}, 322 and 1.3 times higher than those of NH_2-MIL-125(Ti)/0.75CN and NH_2-MIL-125(Ti)/$Ni_{15.8}Pd_{4.1}$, respectively. The enhanced photocatalytic performance can be attributed to the intimate interfacial contact between NH_2-MIL-125(Ti) and CN, accelerating the charge transfer, as well as loaded NiPd nanoparticles, increasing the light-absorbing capacity and accelerating the charge transfer of NH_2-MIL-125(Ti)/CN. This work demonstrates that the addition of appropriate co-catalysts onto MOF/CN hybrid with intimate contact interface provides a new approach to design highly efficient and solar-energy-harvesting photocatalysts.

1. Introduction

Photocatalytic water splitting to produce H_2 is a potential and effective way to store solar energy as chemical energy, and one of the critical issues in this regard is the development of stable and highly efficient photocatalysts [1,2]. To date, many semiconductor materials have been designed for photocatalytic water splitting [3–5]. However, stable photocatalysts with maximum visible-light utilization as well as efficient charge separation for H_2 production have been rarely developed. Metal-organic frameworks (MOFs) are porous crystalline materials connecting inorganic secondary building units (metal ions or clusters) and organic linkers; MOFs have been extensively used as visible-light-driven photocatalysts for H_2 evolution [6–22]. However, these photoactive MOFs still suffer from intrinsic defects such as a low efficiency for solar energy conversion, low conductivity, and fast electron–hole recombination, leading to poor photocatalytic performance compared to traditional inorganic semiconductors [22,23]. Thus, many strategies have been used to improve the photocatalytic activity. For example, combination of MOFs with metal nanoparticles (NPs) [11–16], metal oxides or sulfides [17–19], and dye sensitizers [8,9] has been shown to be effective methods for accelerating the separation of photogenerated charge carriers and preventing the electron–hole recombination, thus leading to improved photocatalytic activity.

Recently, graphitic carbon nitride (g-C_3N_4, CN) has received much attention in various photocatalytic applications as a metal-free polymeric semiconductor because of its remarkable electrical, optical, physiochemical properties, especially its flexible layered structure, making it similar to graphite oxide that can anchor and wrap onto the "host" materials or substrates and thereby creating intimate contact interface between CN and "host" materials [24,25]. Generally, the CN-based composites exhibit improved photocatalytic performance owing to an increased chemical heterogeneity as well as efficient interfacial charge transfer from photoexcited CN to "host" materials. Using MOFs and CN, Wang et al. fabricated Zr-containing MOF (UiO-66)/CN hybrids by thermal annealing. The resulting hybrids showed enhanced photocatalytic H_2 production under visible-light irradiation [10]. Gu et al. developed a highly active electrocatalyst for oxygen reduction reaction using CN-assisted MOFs of CN@NH_2-MIL-101 as the precursor [26]. In addition, coupling of MIL-125(Ti) [27,28] and Cu-BTC [29], NH_2-MIL-88B(Fe) [30], UiO-66 [31], and ZIF-8 [32] with CN improved the

* Corresponding author.
E-mail address: inorchemwl@126.com (L. Wang).

http://dx.doi.org/10.1016/j.apcatb.2017.07.046
0926-3373/

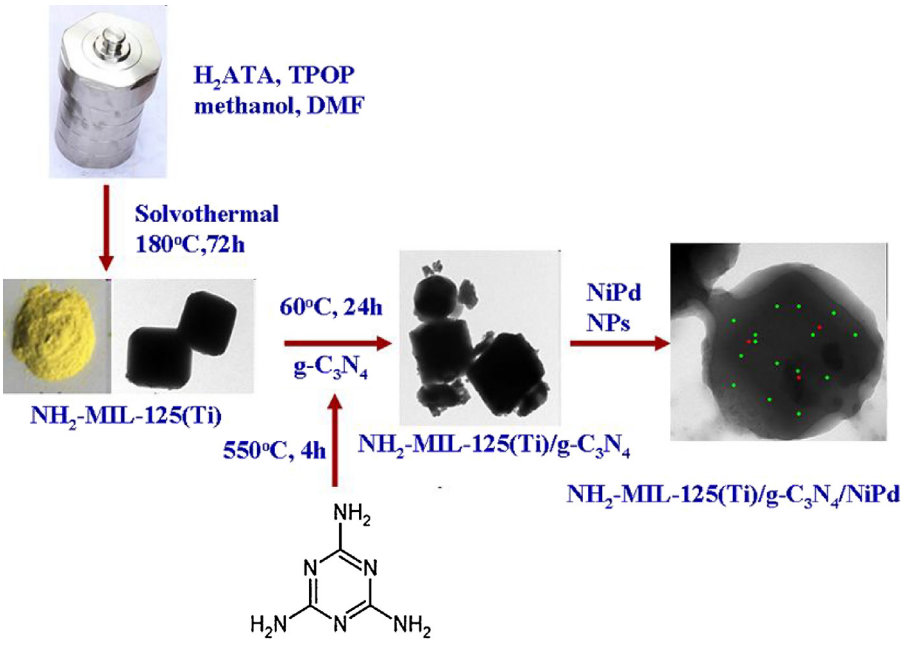

Scheme 1. Illustration for the preparation of NH_2-MIL-125(Ti)/CN/NiPd photocatalyst.

electron–hole separation capabilities and photocatalytic activity of the resulting catalysts.

Alternatively, the integration of an appropriate co-catalyst with strong light-absorbing materials has been used as another strategy to enhance the conversion efficiency of solar energy in H_2 production due to the interface effect as well as localized surface plasmon resonance (SPR) effect [33,34]. In these co-catalysts, the loaded metal NPs acted as efficient media to absorb light, which not only enhanced the visible-light absorption, leading to the generation of more electron–hole pairs, but also facilitated energy transfer to the conduction band (CB) of semiconductor. In addition, a combination of two different novel metal NPs has shown excellent synergistic effects for many photocatalytic applications [35]. For example, Au@CdS/MIL-101 [6], Co@NH_2-MIL-125(Ti) [7], Pt/MIL-101(Cr) [11], Pt@UiO-66-NH2 [8], eosin Y sensitized Ni-Mo/MIL-101 [18], NiRh/MIL-101 [36], NiIr/MIL-101 [37], Au@Pd/UiO-66 (Zr100–*x*Ti*x*) [38], and Ag-Pd/NH_2-UiO-66 [39] have been reported. Typically, Pd-based heterogeneous catalysts have been used in photocatalytic H_2 production [38–42]; noble metal catalysts have been rarely used in practical applications. In this regard, a promising strategy is to fabricate Pd-based alloys with earth-abundant metals, thus not only improving the catalytic activity and selectivity of Pd catalysts but also facilitating the development of cost-effective water splitting photocatalysts. For example, PdCu and PdNi NPs have been used for H_2 evolution reaction [41–43].

Although several MOF/CN composite photocatalysts have been developed for visible-light-driven H_2 production, there are few reports about PdNi bimetallic-decorated MOF/CN heterostructures for H_2 evolution. In addition, the CB potential of a Ti-oxo cluster in NH_2-MIL-125(Ti) is generally considered to be more positive than those of Zr or In counterparts, leading to a more efficient charge transfer from the excited state of the organic linker to the cluster [20]. Therefore, we report a novel heterostructural nanocomposite of NH_2-MIL-125(Ti)/CN/NiPd in this study (Scheme 1). First, NH_2-MIL-125(Ti) was used to anchor CN nanosheets, and then NiPd co-catalysts were deposited on the surface of NH_2-MIL-125(Ti)/CN to form a NH_2-MIL-125(Ti)/CN/NiPd heterostructure. The loaded NiPd co-catalysts served as sensitizers, increasing the light response and improving the photocatalytic efficiency of CN and NH_2-MIL-125(Ti). Moreover, the contact interface between NH_2-MIL-125(Ti)/CN provides a direct path for photoinduced charge transfer, promote the separation of photogenerated electron–hole pairs. Compared to NH_2-MIL-125(Ti), NH_2-MIL-125(Ti)/CN, and NH_2-MIL-125(Ti)/NiPd, the fabricated composites exhibited a higher H_2 evolution rate of 8.7 mmol h^{-1} g^{-1}, 322 times higher than that of NH_2-MIL-125(Ti)/CN. The structure and mechanism of the improved H_2 evolution performance of NH_2-MIL-125(Ti)/CN/NiPd heterostructure were systematically investigated.

2. Experimental

2.1. Preparation of NH_2-MIL-125(Ti)/CN/NiPd heterostructure

2.1.1. Preparation of NH_2-MIL-125(Ti)

NH_2-MIL-125(Ti) was synthesized using a solvothermal method [44]. Typically, 2-aminotetrephthalic acid (H_2ATA, 0.54 g) and tetrapropyl orthotitanate (TPOT, 0.26 mL) were added to a mixture of DMF (9 mL) and methanol (1 mL). The solution was transferred to a Teflon-lined stainless-steel autoclave at 423 K for 72 h. After natural cooling, the yellow precipitate obtained was centrifuged, washed three times with DMF, and dried at 80 °C. The NH_2-MIL-125(Ti) powder obtained was used directly without any further treatment.

2.1.2. Preparation of g-C_3N_4 (CN)

The CN powders were obtained by thermal treatment. Briefly, 10 g of melamine was placed in an alumina crucible with a lid and heated in a muffle furnace at 550 °C for 4 h at a heating rate of 10 °C min^{-1}.

2.1.3. Preparation of NH_2-MIL-125(Ti)/CN hybrid

NH_2-MIL-125(Ti)/CN was fabricated using a self-assembly procedure. First, 0.1 g of NH_2-MIL-125(Ti) was dispersed in 5, 10 mL 15 g L^{-1} CN methanol suspension by ultrasonication for 30 min and stirred at 60 °C for 24 h. After evaporating the methanol, a yellow powder was obtained. The obtained samples were labeled as NH_2-MIL-125(Ti)/0.75CN and NH_2-MIL-125(Ti)/1·5CN according to the weight ratio of CN to NH_2-MIL-125(Ti).

2.1.4. Preparation of NH_2-MIL-125(Ti)/CN/NiPd heterostructure

Ni and Pd NPs were synthesized according to literature [45,46], see Supplementary materials. For the preparation of NH_2-MIL-125(Ti)/CN/NiPd composite, first, 100, 200, and 300 μL of 0.79 mg mL^{-1} Ni (7.9, 15.8, and 23.7 mg g^{-1} of the used NH_2-MIL-125(Ti)/CN, respectively) and 10, 50, 100, and 150 μL of 0.41 mg mL^{-1} Pd (0.41, 2.1, 4.1, and 6.2 mg g^{-1} of the used NH_2-MIL-125(Ti)/CN) were added to 4 mL methanol of NH_2-MIL-125(Ti)/CN (10 mg) under vigorous stirring, and then the mixture was further stirred at room temperature for 12 h. After evaporating the methanol, the catalyst for H_2 production was obtained. The samples were labelled as NH_2-MIL-125(Ti)/CN/Ni*x*Pd*y*, where *x*,*y* denotes the mass ratios of Ni(Pd) to NH_2-MIL-125(Ti)/CN (mg g^{-1}).

2.2. Characterization

Powder X-ray diffraction (XRD) data were collected using a Rigaku D–MAX 2500/PC diffractometer equipped with a Cu Kα radiation source (40 kV, 40 mA). X-ray photoelectron spectra (XPS) were recorded using an X-ray photoelectron spectrometer (Thermo Scientific, Kα) equipped with a monochromatic Al Ka X-ray source (hν = 1486.6 eV). UV–visible diffuse reflectance spectra were recorded using a Lambda 750 UV/VIS/NIR spectrometer. High-resolution transmission electron microscopy (HRTEM) images were recorded using a Tecnai-G^2-F30 high-resolution transmission electron microscope (FEI, USA). A fluorospectrophotometer (F-4500 FL) was used to determine the photoluminescence (PL) spectra. The amounts of NiPd loaded on catalysts were analyzed using a Thermo ICAP-QC inductively coupled plasma optical emission spectroscopy (ICP-MS).

2.3. Photocatalytic activity for H_2 evolution

The photocatalytic reaction was carried out in an 80-mL quartz flask equipped with a flat optical entry window. 10 mg of the photocatalyst was dispersed in 100 mL of an aqueous solution containing 1% of triethanolamine in volume as a sacrificial agent and 0.001 mmol L^{-1} (except for studying the effect of EY concentration on H_2 evolution) of Eosin Y (EY) as the photosensitizer, and the system was deaerated by bubbling N_2 into the solution for 10 min before light irradiation. A 300-W Xe lamp was used as the visible-light source. The amount of H_2 evolved was determined at an interval of 1 h using an online gas chromatography system (GC-7920). The apparent quantum efficiency (AQE) was measured under the same photocatalytic reaction conditions. Photon flux of the incident light was determined using an optical power meter (Model: CEL-NP2000, Beijing China Education Au-Light Co., Ltd). In the AQE test, the reaction mixtures were irradiated for 60 min. AQE was calculated using the following equation:

$$AQE = \frac{2 \times the\ number\ of\ evolved\ hydrogen\ molecules}{the\ number\ of\ incident\ photons} \times 100\%$$

The turnover number (TON) of NiPd for H_2 evolution was calculated using the following equation:

$$TON = \frac{the\ number\ of\ evolved\ hydrogen\ molecules}{the\ number\ of\ Ni\ Pd\ molecules} \times 100\%$$

2.4. Photoelectrochemical measurements

Photocurrent measurements were performed using a CHI 660D electrochemical workstation (Chenhua Instrument, Shanghai, China) in a conventional three-electrode configuration using a Pt foil as the counter electrode and Ag/AgCl (saturated KCl) as the reference electrode. A 300-W Xe arc lamp (PLS-SXE300) was used as the light source. A 0.5 M Na_2SO_4 aqueous solution was used as the electrolyte. The working electrodes were prepared as follows: 5 mg of the prepared photocatalyst was ground with 5 μL of acetylacetone and 500 μL of distilled water for 30 min, making a slurry. The slurry was then spread on an ITO glass substrate with an active area of about 1 × 1 cm^2 using the doctor-blade method and an adhesive tape as the space. The electrode was dried in air and annealed at 200 °C for 30 min under N_2 atmosphere. The photocurrent *vs.* time curve was observed under a constant bias of 1.23 V *vs.* RHE.

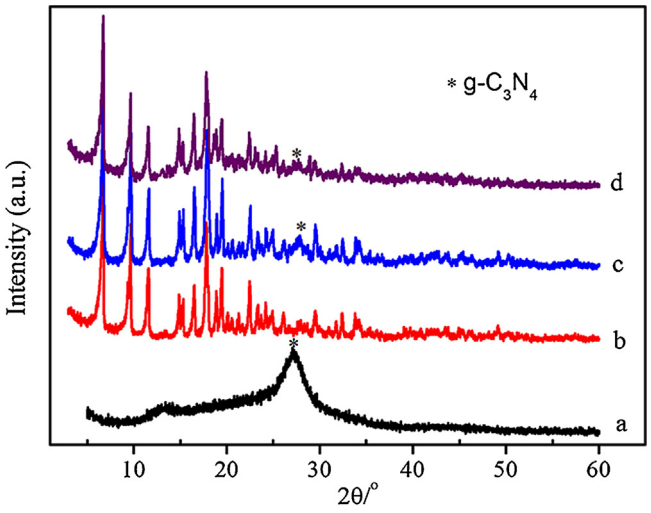

Fig. 1. XRD patterns of the samples of (a) CN, (b) NH_2-MIL-125(Ti), (c) NH_2-MIL-125(Ti)/0.75CN, and (d) NH_2-MIL-125(Ti)/0.75CN/$Ni_{15.8}Pd_{2.1}$ composites.

3. Results and discussion

3.1. Catalyst characterization

Fig. 1 shows the XRD patterns of the as-prepared CN, NH_2-MIL-125(Ti), NH_2-MIL-125(Ti)/0.75CN, and NH_2-MIL-125(Ti)/0.75CN/$Ni_{15.8}Pd_{2.1}$ composites. Pure CN showed two distinct diffraction peaks at 13.3° and 27.2°, corresponding to (100) and (002) planes, respectively [24]. For NH_2-MIL-125(Ti) (Fig. 1b), the main diffraction peaks matched well with those of NH_2-MIL-125(Ti) reported in the literature [12,20], indicating that NH_2-MIL-125(Ti) was successfully synthesized. For NH_2-MIL-125(Ti)/0.75CN/$Ni_{15.8}Pd_{2.1}$ composite, the diffraction peaks of both CN and NH_2-MIL-125(Ti) were detected, indicating that the structure of NH_2-MIL-125(Ti) did not change after hybridization with CN and NiPd co-catalysts. However, no typical diffraction peaks belonging to Ni and Pd were observed (Fig. 1d); this can be mainly attributed to the relatively low content and high dispersion of metal NPs. In addition, the representative peak of CN was not obvious in the XRD pattern of NH_2-MIL-125(Ti)/0.75CN/$Ni_{15.8}Pd_{2.1}$ composite owing to the exfoliation of CN.

Fig. 2 shows the TEM images of NH_2-MIL-125(Ti), CN, NH_2-MIL-125(Ti)/0.75CN, and NH_2-MIL-125(Ti)/0.75CN/$Ni_{15.8}Pd_{2.1}$ samples. The as-prepared NH_2-MIL-125(Ti) has a tetragonal plate morphology with a size of 700 × 200 nm and smooth surface (Fig. 2a), and the CN has a layered structure (Fig. 2b). The surface of NH_2-MIL-125(Ti)/0.75CN particles is less smooth than that of pure NH_2-MIL-125(Ti) (Fig. 2c), indicating that the surface of NH_2-MIL-125(Ti) was encapsulated by CN. Fig. 2d shows the TEM images of NH_2-MIL-125(Ti)/0.75CN/$Ni_{15.8}Pd_{2.1}$ composite. CN was successfully coated on NH_2-MIL-125(Ti), and the contact interface was clearly observed in the TEM image because of different electron penetrability between the CN and NH_2-MIL-125(Ti). This structure can facilitate charge separation and transfer. Moreover, some black small particles of NiPd co-catalysts with a diameter of 4–5 nm were

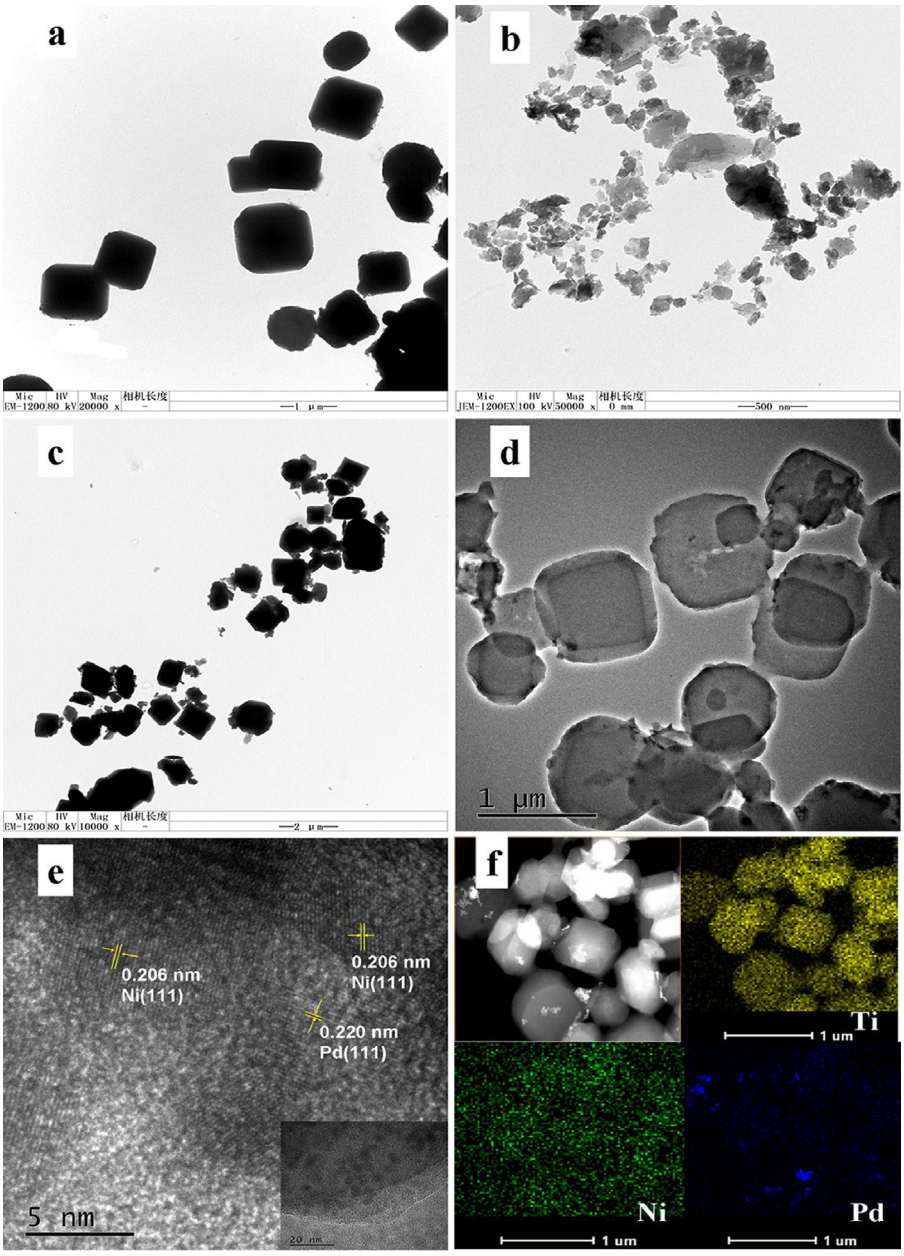

Fig. 2. TEM images of (a) NH_2-MIL-125(Ti), (b) CN, (c) NH_2-MIL-125(Ti)/0.75CN, and (d) NH_2-MIL-125(Ti)/0.75CN/$Ni_{15.8}Pd_{2.1}$; (e) HRTEM image of NiPd NPs; (f) HAADF-STEM image of NH_2-MIL-125(Ti)/0.75CN/$Ni_{15.8}Pd_{2.1}$ composite (scale bar: 200 nm) and STEM-EELS elemental mapping of Ti (yellow), Ni (green), and Pd (blue) distribution on the surface of composite. (For interpretation of the references to colour in this figure legend, the reader is referred to the web version of this article.)

uniformly distributed on the surface of composite (inset in Fig. 2e), and the HRTEM image shows two different types of crystal lattices (Fig. 2e). One lattice fringe spacing is ~0.206 nm, corresponding to the (111) plane of Ni. The other fringe spacing is ~0.220 nm, consistent with the (111) plane of Pd [47]. To confirm the structure of NiPd NPs, a high-angle annular dark-field scanning transmission electron microscopy (HAADF-STEM) image was recorded (Fig. 2f). The STEM-EELS elemental mapping shows that the Pd and Ni singly distributed on the surface of NH_2-MIL-125(Ti)/CN, they cannot form an alloy or core–shell structure, but contact each other partially as shown in Fig. 2e.

The valance states of Pd and Ni atoms on the surface were analyzed by XPS (Fig. S1). The binding energies (BEs) at 873.4 eV and 855.7 eV were assigned to Ni 3p3/2 and Ni 3p1/2, respectively, indicating that the Ni species has Ni(II) oxidation state, and the peak at 861.8 eV confirms the presence of NiO. This result is consistent with that obtained by Luna et al. [48] and can be ascribed to the oxidation of Ni NPs during the drying step in air. In addition, the BE at 853.1 eV reveals the existence of Ni^0. In Fig. S1b, the BEs at 334.5 and 337.7 eV can be attributed to Pd $3d_{5/2}$ and Pd $3d_{3/2}$, respectively, *i.e.*, Pd exists as Pd^0. These results indicate that NH_2-MIL-125(Ti)/CN/NiPd catalyst was successfully obtained.

As illustrated in Fig. 3, pure CN showed an absorption band lower than ~460 nm, resulting in low visible-light utilization efficiency. EY showed an obvious absorption in the range of 200–800 nm, resulting in high UV–vis light utilization efficiency. NH_2-MIL-125(Ti) exhibits two absorption edges extending to ~350 nm and 550 nm, corresponding to the absorption of Ti-O oxo-clusters and ligand-based absorption, respectively [49]. NH_2-MIL-125(Ti)/$Ni_{15.8}Pd_{4.1}$ exhibited significantly enhanced absorption in the visible range beyond the optical response of NH_2-MIL-125(Ti). This can be attributed to the strong absorption

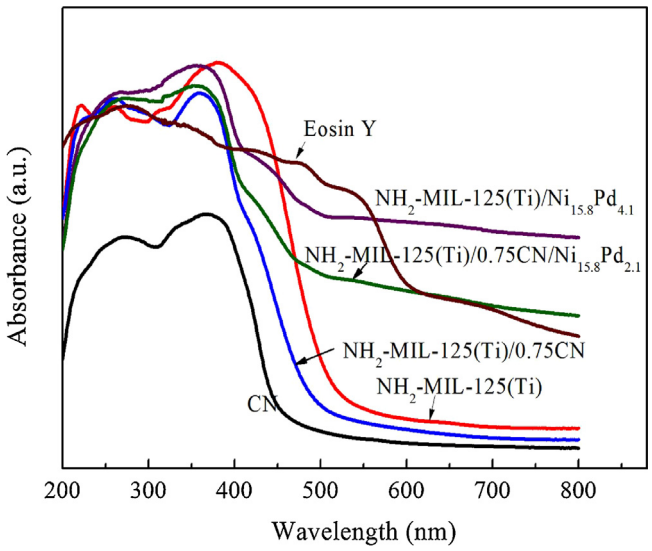

Fig. 3. UV–visible diffuse reflectance spectra of CN, EY, NH_2-MIL-125(Ti), NH_2-MIL-125(Ti)/0.75CN, NH_2-MIL-125(Ti)/$Ni_{15.8}Pd_{4.1}$ and NH_2-MIL-125(Ti)/0.75CN/$Ni_{15.8}Pd_{2.1}$ heterostructures.

in the visible-light range of NiPd co-catalysts [50,51]. Moreover, NH_2-MIL-125(Ti)/$Ni_{15.8}Pd_{4.1}$ composite showed a more enhanced visible-light absorption than NH_2-MIL-125(Ti)/$Pd_{4.1}$ and NH_2-MIL-125(Ti)/$Ni_{15.8}$ (Fig. S2). After attaching CN onto NH_2-MIL-125(Ti), a blue-shifted absorption edge was observed for the NH_2-MIL-125(Ti)/0.75CN and NH_2-MIL-125(Ti)/0.75CN/$Ni_{15.8}Pd_{2.1}$ samples. The absorbance spectrum of NH_2-MIL-125(Ti)/0.75CN/$Ni_{15.8}Pd_{2.1}$ showed a combination of the spectral features of pure CN, NiPd, and NH_2-MIL-125(Ti), exhibiting an extended absorption edge and stronger visible-light absorption. So in the reaction process of photocatalysis H_2 evolution in EY-sensitized NH_2-MIL-125(Ti)/CN/NiPd system, the added EY and loaded NiPd may be offer the catalyst ability using longer wavelength visible light in a majority of the solar spectrum.

3.2. Catalytic performance

Photocatalytic H_2 evolution of the as-prepared samples was evaluated in the presence of triethanolamine (a sacrificial agent) and EY (photosensitizer). No appreciable H_2 evolution was detected over NH_2-MIL-125(Ti) and NH_2-MIL-125(Ti)/$Ni_{15.8}$ without Pd deposition. However, as shown in Fig. 4a, all the NiPd-deposited NH_2-MIL-125(Ti) samples exhibited much higher H_2 evolution activities than monometallic NP-supported NH_2-MIL-125(Ti) owing to the synergistic effect of Ni and Pd. As shown in Figs. S4 and S5, the work functions of Ni (111) and Pd (111) were 4.993 and 4.855 eV, respectively. The Fermi energy of the Pd (111) surface was lower than that of the Ni (111) surface. The Ni NPs contact with the Pd NPs as shown in HRTEM (Fig. 2e), favoring the photogenerated electron transfer from Ni to Pd because of different Fermi energies, leading to efficient charge separation and improving H_2 production. Specifically, the rate of H_2 production of NH_2-MIL-125(Ti)/$Ni_{7.9}Pd_{4.1}$ reached 5.22 mmol g^{-1} h^{-1}, 5.1 times higher than that of Ti-MOF/$Pd_{4.2}$ (1.02 mmol g^{-1} h^{-1}). The rate of H_2 production over NH_2-MIL-125(Ti)/$Ni_{15.8}Pd_{4.1}$ reached 6.81 mmol g^{-1} h^{-1}, 6.7-fold of that of NH_2-MIL-125(Ti)/$Pd_{4.1}$. Here, the amounts of Ni and Pd NPs loaded on catalyst measured by ICP-MS were 2.339 and 0.297 mmol g^{-1}, respectively. The amount of H_2 evolved over NH_2-MIL-125(Ti)/$Ni_{15.8}Pd_{4.1}$ for 9 h was 61.325 mmol g^{-1}. This corresponds to a TON of 23.2 mol_{H2}/mol_{NiPd} (Table S1). A further increase in the Ni:Pd loading amount (23.7:4.1) decreased the rate of H_2 production (5.06 mmol g^{-1} h^{-1}). By taking the optimal loading amount of Ni:Pd (15.8:4.1) as a benchmark, different coating amounts of CN (0, 5, and 10 mL) onto NH_2-MIL-125(Ti) were investigated to determine their effects on H_2 evolution rate. As shown in Fig. 4b, upon the coating of 0.75% CN (as NH_2-MIL-125(Ti)/0.75CN/$Ni_{15.8}Pd_{4.1}$) onto the NH_2-MIL-125(Ti) surfaces, the rate of H_2 production increased from 6.81 mmol g^{-1} h^{-1} to 7.84 mmol g^{-1} h^{-1}. Control experiments indicated that a slight amount of H_2 (133 μmol g^{-1}) was evolved from NH_2-MIL-125(Ti)/0.75CN before the quenching (Fig. S6). These results confirm that the formation of NH_2-MIL-125(Ti)/CN heterojunctions (Fig. 2d, TEM image) leads to larger interfaces, thus achieving a more effective separation of photogenerated electrons and holes for enhanced photocatalytic activities. After the coating of 1.5% CN onto NH_2-MIL-125(Ti) (as NH_2-MIL-125(Ti)/1.5CN/$Ni_{15.8}Pd_{4.1}$) surface, the rate of H_2 production decreased (5.72 mmol g^{-1} h^{-1}). This is because excess CN weakened the charge transfer between CN and NH_2-MIL-125(Ti). Similar result was observed for MOF (UiO-66)/CN system [10].

Control experiments showed that small amounts of H_2 (53.05 and 1.91 mmol g^{-1}) were generated over NH_2-MIL-125(Ti)/0.75CN/$Ni_{15.8}$ and NH_2-MIL-125(Ti)/0.75CN/$Pd_{4.1}$ before the quenching, respectively, indicating that the enhanced activity of NH_2-MIL-125(Ti)/0.75CN/$Ni_{15.8}Pd_{4.1}$ (97.84 mmol g^{-1} within 15 h) can be attributed to the synergistic effect between Ni and Pd. However, Pd is a precious metal; therefore, a suitable ratio of Ni to Pd in photocatalysts with excellent H_2 production performance has always been a concern for economic applications. Thus, by taking the optimal result of NH_2-MIL-125(Ti)/0.75CN as a benchmark, different doping amounts of Pd (0.41, 2.1, 4.1, and 6.2 mg g^1) with 15.8 mg g^{-1} Ni onto NH_2-MIL-125(Ti)/0.75CN were investigated to determine their effects on H_2 evolution rate. Even when a small amount of Pd (0.41 mg g^{-1}) was added, the rate of H_2 production over NH_2-MIL-125(Ti)/0.75CN/$Ni_{15.8}Pd_{0.41}$ was 4.59 mmol g^{-1} h^{-1} with a TON of 17.9 mol_{H2}/mol_{NiPd}. The H_2 evolution rate reached 8.70 mmol g^{-1} h^{-1} when the amount of Pd was increased to 2.1 mg g^{-1}, *i.e.*, NH_2-MIL-125(Ti)/0.75CN/$Ni_{15.8}Pd_{2.1}$, 7.2 times higher than that of NH_2-MIL-125(Ti)/0.75CN/$Pd_{4.1}$. The TON increased to 32.4 mol_{H2}/mol_{NiPd}, and the AQE of 6.8% was achieved (Table S2). A further increase in the Pd loading amount to 4.1 and 6.2 mg g^{-1} decreased the H_2 evolution rate (7.84 and 7.07 mmol g^{-1} h^{-1}, respectively) with a decreased TON (27.6 and 24.5 mol_{H2}/mol_{NiPd}, respectively). In addition, the H_2 evolution rate over NH_2-MIL-125(Ti)/0.75CN/$Ni_{15.8}Pd_{2.1}$ increased with an increase in the EY concentration (Fig. 4d), and a small value of 0.058 mmol g^{-1} h^{-1} was observed for NH_2-MIL-125(Ti)/0.75CN/$Ni_{15.8}Pd_{2.1}$ without adding EY. According to the UV–vis absorption spectra of EY solution (10^{-4} mol L^{-1}), the highest absorption wavelength of EY was 516 nm (Fig. S7). Thus, the H_2 evolution rate over NH_2-MIL-125(Ti)/0.75CN/$Ni_{15.8}Pd_{2.1}$ at 520 nm was determined to investigate the EY wavelength dependence of photocatalytic H_2 activity, and a value of 4.45 mmol g^{-1} h^{-1} was obtained with an AQE of 85.7%. These results indicate that the H_2 evolution reaction was indeed driven by the input light adsorbed by EY [52].

The stability of NH_2-MIL-125(Ti)/0.75CN/$Ni_{15.8}Pd_{2.1}$ for H_2 evolution was evaluated by performing recycling experiments under visible-light irradiation. At the end of each run, the reaction cell was vacuumed to remove the H_2 produced. As shown in Fig. 5, NH_2-MIL-125(Ti)/0.75CN/$Ni_{15.8}Pd_{2.1}$ shows considerable durability in the third consecutive run. The amount of H_2 evolved from NH_2-MIL-125(Ti)/0.75CN/$Ni_{15.8}Pd_{2.1}$ is ~104.65 mmol g^{-1} in the total 20-h recycle experiment. This result indicates that NH_2-MIL-125(Ti)/0.75CN/$Ni_{15.8}Pd_{2.1}$ heterostructure had good stability in photocatalytic H_2 evolution from water.

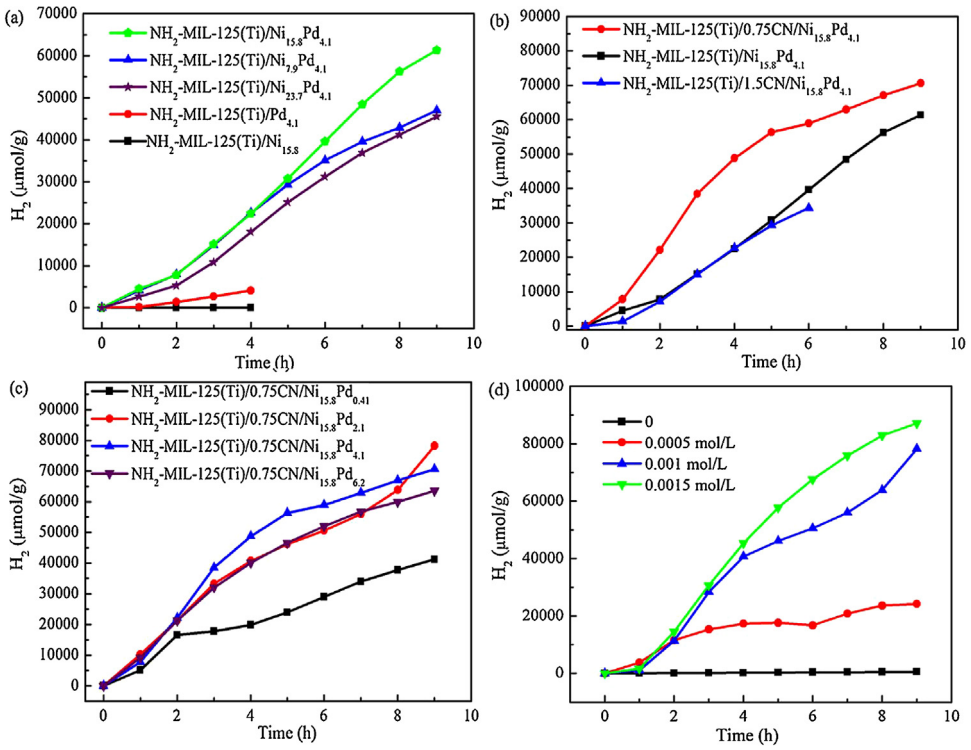

Fig. 4. (a) H_2 evolution amounts over various NH_2-MIL-125(Ti)/NiPd hybrids with various amounts of NiPd. (b) Effect of amount of CN coated onto NH_2-MIL-125(Ti)/$Ni_{15.8}Pd_{4.1}$. (c) Effect of Pd dosage deposited onto NH_2-MIL-125(Ti)/0.75CN/$Ni_{15.8}$. (d) Effects of EY dosage on H_2 evolution under 9 h visible-light irradiation. Reaction conditions: $m_{catalyst}$ = 10 mg, T = 25 °C, and light.
Source: 300-W Xe lamp.

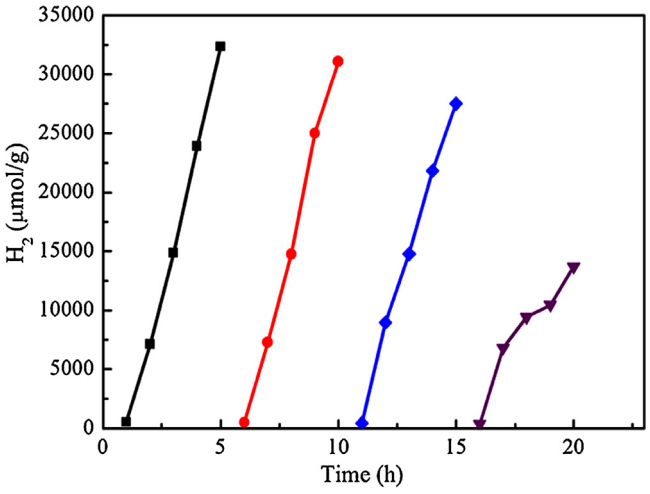

Fig. 5. Stability measurements of the amount of H_2 evolved under visible-light irradiation over NH_2-MIL-125(Ti)/0.75CN/$Ni_{15.8}Pd_{2.1}$ photocatalyst.

3.3. Mechanism

First, photocurrent measurements were carried out to determine the charge-separation efficiency. As shown in Fig. 6a, the photocurrent density of NH_2-MIL-125(Ti) and NH_2-MIL-125(Ti)/0.75CN electrodes (curves a and b) reached 0.5 and 0.7 μA cm^{-2}, respectively. The enhanced photocurrent density of NH_2-MIL-125(Ti)/0.75CN can be attributed to the heterostructure between NH_2-MIL-125(Ti) and CN that increased the transfer and separation efficiency of photogenerated charges [10,27]. After the introduction of NiPd co-catalysts onto NH_2-MIL-125(Ti)/0.75CN, the photocurrent density was improved, and NH_2-MIL-125(Ti)/0.75CN/$Ni_{15.8}Pd_{2.1}$ composite showed a photocurrent density of 0.9 μA cm^{-2}. This further confirmed that NiPd NPs served as an effective co-catalyst, accelerating the separation of photogenerated charges and improving the performance of photocatalytic H_2 evolution [33,36,37]. The improved charge separation of photogenerated electron–hole pairs in NH_2-MIL-125(Ti)/0.75CN/$Ni_{15.8}Pd_{2.1}$ composite was further confirmed from the PL spectra. As shown in Fig. 6b, pristine NH_2-MIL-125(Ti) and CN showed strong PL emission peaks centered at ~470 and 458 nm, respectively. Notably, the coating of CN onto NH_2-MIL-125(Ti) (NH_2-MIL-125(Ti)/0.75CN) weakened the PL peak intensity, indicating charge transfer between NH_2-MIL-125(Ti) and CN. Such a rapid charge transfer indicates the intimate contact between CN and NH_2-MIL-125(Ti), as shown by the HRTEM image (Fig. 2d). The PL peak intensity further decreased when the NiPd co-catalysts were deposited onto the surface of NH_2-MIL-125(Ti)/0.75CN. These observations indicate that the photoinduced electron–hole recombination was more effectively suppressed when a heterojunction was formed among NH_2-MIL-125(Ti), CN, and NiPd co-catalyst.

Based on the above discussion, a tentative mechanism for the photocatalytic H_2 production over NH_2-MIL-125(Ti)/CN/NiPd composite is proposed, As shown in Scheme 2, the absorbed EY on the surface of NH_2-MIL-125(Ti)/CN/NiPd absorbs light photons to form a singlet excited state EY^{1*}, and then forms EY^{3*} by intersystem crossing (ISC). EY^{3*} can be quenched by TEOA to produce $EY^{\bullet-}$ [14,53–55], and electrons are then transferred from $EY^{\bullet-}$ to the Ti-oxo clusters, the CB of CN, or the loaded NiPd co-catalysts directly. Additionally, CN can also be excited to generate electrons. Because the CB edge of CN (−0.92 eV *vs.* NHE) is more negative than that of NiO (−0.5 V *vs.* NHE), the photoexcited electrons on CN surface are injected into the loaded NiPd where the protons are reduced to form molecular H_2. On the other hand, upon photon absorption by the ligand H_2ATA, the photogenerated and injected

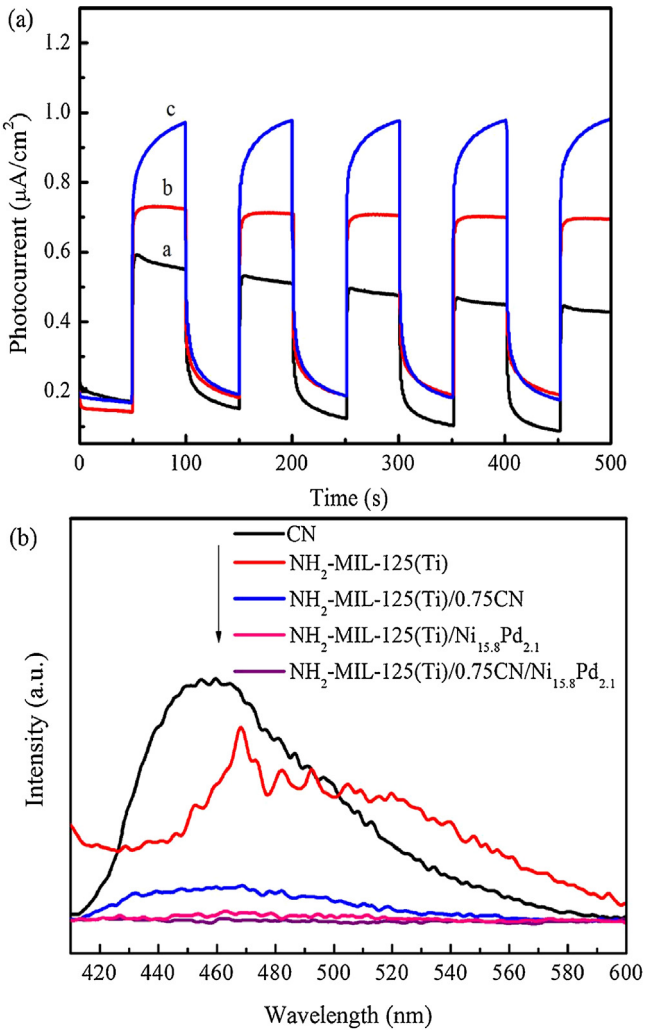

Fig. 6. (a) Photocurrent and (b) photoluminescence spectra of the obtained samples.

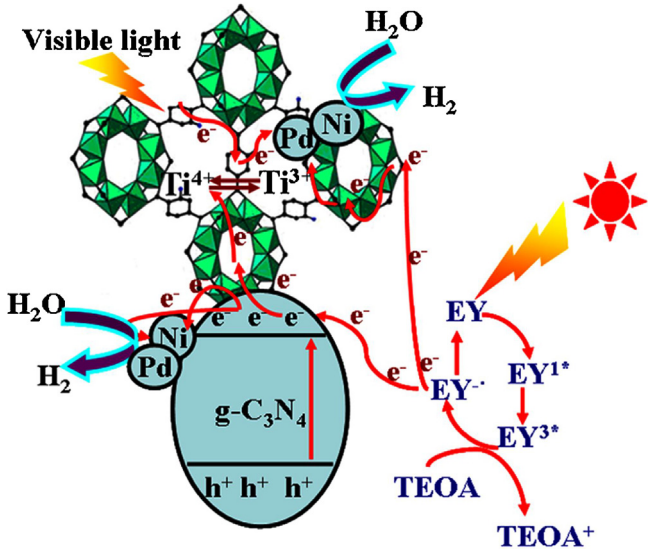

Scheme 2. Mechanism of H_2 evolution reaction over EY-sensitized NH_2-MIL-125(Ti)/CN/NiPd under visible illumination.

electrons originating from the CB of CN or $EY^{\bullet -}$ are transferred to the Ti^{4+} in the Ti–O (Ti oxo) cluster to generate Ti^{3+}. The presence of Ti^{3+} in the Ti oxo-clusters of NH_2-MIL-125(Ti) explains the color change from bright yellow to green in the presence of N_2 upon visible-light irradiation. The close interfacial connections between CN and NH_2-MIL-125(Ti) are responsible for such an electron transfer [26]. As a result, the photoinduced electrons and holes are further separated in space, thus hindering the recombination of electron–hole pairs and improving the photoactivity. Finally, the protons accumulated on the surface of NH_2-MIL-125(Ti)/CN are transferred to the NiPd co-catalysts and react with electrons to produce H_2. The holes remaining within the valence band of CN and organic linker are consumed by TEOA, which acts as an electron donor. The electron migration pathway was evidenced by the decreased PL intensity of NH_2-MIL-125(Ti)/0.75CN or NiPd-loaded NH_2-MIL-125(Ti)/0.75CN.

Control experiments showed that smaller amounts of H_2 (2.86 mmol g^{-1}) were generated over CN/$Ni_{15.8}Pd_{2.1}$ before the quenching. Therefore, the role of NH_2-MIL-125(Ti) in the improvement of H_2 evolution performance can be attributed to the following reasons: (1) NH_2-MIL-125(Ti) has a large specific surface area favoring the formation of a heterostructure between NH_2-MIL-125(Ti) and CN with intimate contact interface and allows the well-dispersion of NiPd co-catalysts. (2) The porous MOFs serve as electric conductors to promote the electron transfer in facilitating the separation of photoelectrons from CN and EY. (3) The MOFs act as photoelectron generators to enhance the activity of H_2 production.

4. Conclusions

In summary, novel visible-light-driven photocatalysts were successfully fabricated by coating two-dimensional (2D) CN nanosheets on NH_2-MIL-125(Ti), followed by depositing NiPd co-catalysts onto NH_2-MIL-125(Ti)/CN surface, thus forming a heterostructural composite. Compared to monometallic-based (Ni and Pd) photocatalysts, NH_2-MIL-125(Ti)/CN/$Ni_{15.8}Pd_{2.1}$ heterostructure exhibited the highest photocatalytic activity after sensitizing with EY with a H_2 evolution rate of 8.7 mmol g^{-1} h^{-1}. The enhanced photocatalytic performance can be attributed to the efficient interfacial charge transfer from CN to NH_2-MIL-125(Ti), the strong light-absorbing and charge transfer capacities of NiPd co-catalysts. This study provides a promising way to construct highly efficient MOF-based heterostructural photocatalysts.

Acknowledgements

The authors would like to thank the National Natural Science Foundation of China (No 51404143) and Shandong Provincial Natural Science Foundation, China (2015ZRB01A0D).

Appendix A. Supplementary data

Supplementary data associated with this article can be found, in the online version, at http://dx.doi.org/10.1016/j.apcatb.2017.07.046.

References

[1] N.S. Lewis, D.G. Nocera, Proc. Natl. Acad. Sci. U. S. A. 103 (2006) 15729–15735.
[2] X.Y. Ma, J.Q. Li, C.H. An, J. Feng, Y.H. Chi, J.X. Liu, J. Zhang, Y.G. Sun, Nano Res. 9 (2016) 2284–2293.
[3] J.R. Ran, J. Zhang, J.G. Yu, M. Jaroniec, S.Z. Qiao, Chem. Soc. Rev. 43 (2014) 7787–7812.
[4] F.E. Osterloh, Chem. Soc. Rev. 42 (2013) 2294–2320.
[5] A.I. Hochbaum, P.D. Yang, Chem. Rev. 110 (2010) 527–546.

[6] J.S. Zhao, Y. Wang, J.W. Zhou, P.F. Qi, S.W. Li, K.X. Zhang, X. Feng, B. Wang, C.W. Hu, J. Mater. Chem. A 4 (2016) 7174–7177.
[7] C.W. Zhao, Y.A. Li, X.R. Wang, G.J. Chen, Q.K. Liu, J.P. Ma, Y.B. Dong, Chem. Commun. 51 (2015) 15906–15909.
[8] Y.P. Yuan, L.S. Yin, S.W. Cao, G.S. Xu, C.H. Li, C. Xue, Appl. Catal. B: Environ. 168–169 (2015) 572–576.
[9] X.L. Liu, R. Wang, M.Y. Zhang, Y.P. Yuan, C. Xue, APL Mater. 3 (2015) 104403–104409.
[10] R. Wang, L.N. Gu, J.J. Zhou, X.L. Liu, F. Teng, C.H. Li, Y.H. Shen, Y.P. Yuan, Adv. Mater. Interfaces 2 (2015) 1500037–1500041.
[11] Y.J. Wang, Y.N. Zhang, Z.Q. Jiang, G.Y. Jiang, Z. Zhao, Q.H. Wu, Y. Liu, Q. Xu, A.J. Duan, C.M. Xu, Appl. Catal. B: Environ. 185 (2016) 307–314.
[12] M.A. Nasalevich, R. Becker, E.V. Ramos-Fernandez, S. Castellanos, S.L. Veber, M.V. Fedin, F. Kapteijn, J.N.H. Reek, J.I. van der Vlugt, J. Gascon, Energy Environ. Sci. 8 (2015) 364–375.
[13] J.D. Xiao, Q.C. Shang, Y.J. Xiong, Q. Zhang, Y. Luo, S.H. Yu, H.L. Jiang, Angew. Chem. 128 (2016) 9535–9539.
[14] W.L. Zhen, H.B. Gao, B. Tian, J.T. Ma, G.X. Lu, ACS Appl. Mater. Interfaces 8 (2016) 10808–10819.
[15] M.C. Wen, Y. Kuwahara, K. Mori, D.Q. Zhang, H.X. Li, H. Yamashita, J. Mater. Chem. A 3 (2015) 14134–14141.
[16] M.C. Wen, K. Mori, T. Kamegawa, H. Yamashita, Chem. Commun. 50 (2014) 11645–11648.
[17] Y. Su, Z. Zhang, H. Liu, Y. Wang, Appl. Catal. B: Environ. 200 (2017) 448–457.
[18] L.J. Shen, M.B. Luo, Y.H. Liu, R.W. Liang, F.F. Jing, L. Wu, Appl. Catal. B: Environ. 166–167 (2015) 445–453.
[19] Y.H. Bu, F.Y. Li, Y.Z. Zhang, R. Liu, X.Z. Luo, L. Xu, RSC Adv. 6 (2016) 40560–40566.
[20] Y. Horiuchi, T. Toyao, M. Saito, K. Mochizuki, M. Iwata, H. Higashimura, M. Anpo, M. Matsuoka, J. Phys. Chem. C 116 (2012) 20848–20853.
[21] A. Dhakshinamoorthy, A.M. Asiri, H. García, Angew. Chem. 55 (2016) 5414–5445.
[22] K. Meyer, M. Ranocchiari, J.A. van Bokhoven, Energy Environ. Sci. 8 (2015) 1923–1937.
[23] C.C. Wang, J.R. Li, X.L. Lv, Y.Q. Zhang, G.S. Guo, Energy Environ. Sci. 7 (2014) 2831–2867.
[24] W.J. Ong, L.L. Tan, Y.H. Ng, S.T. Yong, S.P. Chai, Chem. Rev. 116 (2016) 7159–7329.
[25] J.Q. Wen, J. Xie, X.B. Chen, X. Li, Appl. Surf. Sci. 391 (2017) 72–123.
[26] W.L. Gu, L.Y. Hu, J. Li, E. Wang, ACS Appl. Mater. Interfaces 8 (2016) 35281–35288.
[27] Z.W. Yang, X.Q. Xu, X.X. Liang, C. Lei, Y.H. Cui, W.H. Wu, Y.X. Yang, Z. Zhang, Z.Q. Lei, Appl. Catal. B: Environ. 205 (2017) 42–54.
[28] H. Wang, X.Z. Yuan, Y. Wu, G.M. Zeng, X.H. Chen, L.J. Leng, H. Li, Appl. Catal. B: Environ. 174–175 (2015) 445–454.
[29] A.D. Giannakoudakis, N.A. Travlou, J. Secor, T.J. Bandosz, Small 13 (2017) 1601758–1601766.
[30] X.Y. Li, Y.H. Pi, L.Q. Wu, Q.B. Xia, J.L. Wu, Z. Li, J. Xiao, Appl. Catal. B: Environ. 202 (2017) 653–663.
[31] L. Shi, T. Wang, H.B. Zhang, K. Chang, J.H. Ye, Adv. Funct. Mater. 25 (2015) 5360–5367.
[32] S. Panneri, M. Thomas, P. Ganguly, B.N. Nair, A.P. Mohamed, K.G.K. Warrier, U.S. Hareesh, Catal. Sci. Technol. 7 (2017) 2118–2128.
[33] J.J. Ding, X.Y. Li, L. Chen, X. Zhang, S. Sun, J. Bao, C. Gao, X.Y. Tian, J. Mater. Chem. A 4 (2016) 12630–12637.
[34] X.B. Wei, C.L. Shao, X.H. Li, N. Lu, K.X. Wang, Z.Y. Zhang, Y.C. Liu, Nanoscale 8 (2016) 11034–11043.
[35] A.K. Singh, Q. Xu, ChemCatChem 5 (2013) 652–676.
[36] P.P. Zhao, N. Cao, W. Luo, G.Z. Cheng, J. Mater. Chem. A 3 (2015) 12468–12475.
[37] P.P. Zhao, N. Cao, J. Su, W. Luo, G.Z. Cheng, ACS Sustain. Chem. Eng. 3 (2015) 1086–1093.
[38] M.C. Wen, K. Mori, Y. Kuwahara, H. Yamashita, ACS Energy Lett. 2 (2017) 1–7.
[39] S.T. Gao, W.H. Liu, C. Feng, N.Z. Shang, C. Wang, Catal. Sci. Technol. 6 (2016) 869–874.
[40] Z. Zhang, S. Cao, Y. Liao, C. Xue, Appl. Catal. B: Environ. 162 (2015) 204–209.
[41] M. Ren, Y. Zhou, F. Tao, Z. Zou, D.L. Akins, H. Yang, J. Phys. Chem. C 118 (2014) 12669–12675.
[42] K. Mori, H. Tanaka, M. Dojo, K. Yoshizawa, H. Yamashita, Chem. Eur. J. 21 (2015) 12085–12092.
[43] H. Husin, W.N. Su, C.J. Pan, J.Y. Liu, J. Rick, S.C. Yang, W.T. Chuang, H.S. Sheu, B.J. Hwang, Int. J. Hydrogen Energy 38 (2013) 13529–13540.
[44] M. Dan-Hardi, C. Serre, T. Frot, L. Rozes, G. Maurin, C. Sanchez, G.J. Feírey, J. Am. Chem. Soc. 131 (2009) 10857–10859.
[45] Y.Z. Chen, D.L. Peng, D.X. Lin, X.H. Luo, Nanotechnology 18 (2007) 505703–505708.
[46] K. Jiang, H.X. Zhang, Y.Y. Yang, R. Mothes, H. Lang, W.B. Cai, Chem. Commun. 47 (2011) 11924–11926.
[47] L.J. Liu, R.F. Chen, W.K. Liu, J.M. Wu, D. Gao, J. Hazard. Mater. 320 (2016) 96–104.
[48] A.L. Luna, E. Novoseltceva, E. Louarn, P. Beaunier, E. Kowalska, B. Ohtani, M.A. Valenzuela, H. Remita, C. Colbeau-Justin, Appl.Catal. B: Environ. 191 (2016) 18–28.
[49] Y. Fu, D. Sun, Y. Chen, R. Huang, Z. Ding, X. Fu, Z. Li, Angew. Chem. Int. Ed. 51 (2012) 3364–3367.
[50] L.M. Song, S.J. Zhang, J. Hazard. Mater. 174 (2010) 563–566.
[51] J.L. Zhang, Y. Lu, L. Ge, C.C. Han, Y.J. Li, Y.Q. Gao, S.S. Li, H. Xu, Appl. Catal. B: Environ. 204 (2017) 385–393.
[52] W.L. Zhen, J.T. Ma, G.X. Lu, Appl. Catal. B: Environ. 190 (2016) 12–25.
[53] W. Zhang, J. Hong, J. Zheng, Z. Huang, J. Zhou, R. Xu, J. Am. Chem. Soc. 133 (2011) 20680–20683.
[54] D. Wang, M. Gong, H. Chou, C. Pan, H. Chen, Y. Wu, M. Lin, M. Guan, J. Yang, C. Chen, Y. Wang, B.J. Hwang, C. Chen, H. Dai, J. Am. Chem. Soc. 137 (2015) 1587–1592.
[55] T. Lazarides, T. McCormick, P. Du, G. Luo, B. Lindley, R. Eisenberg, J. Am. Chem. Soc. 131 (2009) 9192–9194.